Why can water cages adsorb aqueous methane? A potential of mean force calculation on hydrate nucleation mechanisms

Guang-Jun Guo,*[a] Meng Li,[a] Yi-Gang Zhang[b] and Chang-Hua Wu[b]

Received 13th July 2009, Accepted 15th September 2009
First published as an Advance Article on the web 6th October 2009
DOI: 10.1039/b913898f

By performing constrained molecular dynamics simulations in the methane–water system, we successfully calculated the potential of mean force (PMF) between a dodecahedral water cage (DWC) and dissolved methane for the first time. As a function of the distance between DWC and methane, this is characterized by a deep well at $\sim$6.2 Å and a shallow well at $\sim$10.2 Å, separated by a potential barrier at $\sim$8.8 Å. We investigated how the guest molecule, cage rigidity and the cage orientation affected the PMF. The most important finding is that the DWC itself strongly adsorbs methane and the adsorption interaction is independent of the guests. Moreover, the activation energy of the DWC adsorbing methane is comparable to that of hydrogen bonds, despite differing by a factor of $\sim$10% when considering different water–methane interaction potentials. We explain that the cage–methane adsorption interaction is a special case of the hydrophobic interaction between methane molecules. The strong net attraction in the DWC shell with radii between 6.2 and 8.8 Å may act as the inherent driving force that controls hydrate formation. A cage adsorption hypothesis for hydrate nucleation is thus proposed and discussed.

Introduction

Gas hydrates have attracted significant attention because of their importance to energy resources, the environment, flow assurance and geological disaster prevention.[1–5] Among them, methane hydrate is the most common and has been studied widely. By pressurizing gaseous methane in liquid water at a low temperature, the ice-like methane hydrate is obtained, with a chemical formula $CH_4{\cdot}5.75H_2O$.[6] It has the sI clathrate structure, in which methane molecules (guests) are trapped in dodecahedral (5^{12}) and tetrakaidecahedral ($5^{12}6^2$) cages. These cages are composed of water molecules (hosts) that link to one another through hydrogen bonds and tessellate the three-dimensional space by sharing their faces with each other. The chemical reaction for forming the hydrate involves many puzzling features. For example, the solubility of methane in water is very low ($\sim 10^{-3}$ mole fraction[7]) but it is enhanced by two orders of magnitude in hydrates and no chemical bond forms between the two types of molecule. Moreover, the reaction requires an induction time and shows a widely observed, but still poorly understood, ''memory effect''.[8] To resolve these puzzles, the hydrate formation mechanism, especially the initial nucleation pathway, should be investigated in detail on a molecular level.

Various ideas have been proposed for hydrate nucleation. They mainly include the labile cluster hypothesis, proposed by Sloan's group,[6,9,10] emphasizing the aggregation of cage-like water clusters (*i.e.*, the solvation shells of the gas molecule) and the local structuring hypothesis, proposed by Trout's group,[11] emphasizing the adjustment of water molecules around a local, ordered arrangement of gas molecules. Recently, by measuring the lifetime of a dodecahedral water cage (DWC) immersed in bulk water,[12] we found that the DWC can adsorb dissolved methane and its lifetime increases exponentially with the number of adsorbed methane molecules. We thus proposed that methane molecules aggregating in this way favors hydrate nucleation. De Pablo's group[13] also measured the cage lifetime at the water–methane interface and found that it almost doubles the cage lifetime in bulk water; their work supports our model. However, based on hydrate nucleation simulations at the water–methane interface, Rodger's group[14,15] observed that the initial nucleus looks like a complex packing of cages and concluded that the processes of cage formation and methane adsorption in our model are concurrent rather than consecutive. In other words, cage formation correlates strongly with the collective arrangement of methane molecules, thus supporting the local structuring hypothesis.[11] We believe it is not substantial to argue whether these processes are concurrent or consecutive. The most crucial question is to explain the intrinsic driving forces that control them.

The methane adsorption phenomenon often appears in MD simulation studies on hydrates but it is still poorly understood. Much evidence[16–18] shows that methane molecules are adsorbed on the surface cages of methane hydrate during hydrate dissociation and growth processes. We inserted a DWC into a dilute methane solution and found that the DWC could trap methane diffusing freely in water.[12] Generally speaking, because the DWC has been filled with a methane molecule, methane adsorption should mainly be

[a] *Key Laboratory of the Earth's Deep Interior, Institute of Geology and Geophysics, Chinese Academy of Sciences, Beijing 100029, People's Republic of China. E-mail: guogj@mail.igcas.ac.cn*
[b] *State Key Laboratory of Lithospheric Evolution, Institute of Geology and Geophysics, Chinese Academy of Sciences, Beijing 100029, People's Republic of China*

caused by solvent-induced hydrophobic interactions between the caged methane and the free methane together with direct attractive forces between them. However, this explanation is not certain. It is well known that the radius distribution function (RDF) between methane molecules in liquid water, denoted as $g_{MM}(r)$, shows three peaks located at about 3.9, 7.1 and 10.2 Å.[12,19–22] The first peak represents the contact methane pair while the second corresponds to the solvent-separated pair. However, we observed that the preferential distance between the DWC center and the adsorbed methane, r_{adsorb}, is 6.15 Å,[12] beyond the location of the first minimum of $g_{MM}(r)$, 5.4 Å. Therefore, if methane adsorption were only ascribed to the hydrophobic interactions between methane molecules, r_{adsorb} would be around 7.1 Å, rather than 6.15 Å. There must therefore be an additional attractive interaction between the DWC and the adsorbed methane. If so, the intrinsic driving force controlling hydrate nucleation must be reconsidered. A straightforward method to verify this conjecture is to check the RDF between an empty DWC and a dissolved methane, denoted as $g_{DWC-M}(r)$. If an extra attractive interaction does exist, the peak at r_{adsorb} will still appear and, if not, it will disappear because all interactions between methanes have been removed.

However, obtaining an accurate $g_{DWC-M}(r)$ is a difficult task. Direct calculation of the distribution of the distance between DWC and methane is infeasible because of the low solubility of methane in water, leading to the problem of poor sampling. Using this method together with hand-sampling, we obtained a qualitative $g_{DWC-M}(r)$,[12] that is, a sharp peak located at 6.15 Å but of uncertain height. Alternatively, one can indirectly calculate the $g_{DWC-M}(r)$ from the potential of mean force (PMF) between DWC and methane through the relationship,

$$g(r) = e^{-PMF(r)/k_B T} \quad (1)$$

where k_B is the Boltzmann constant and T is the system temperature. The calculation of PMF requires heavy computational effort and this is the challenge addressed in the present work.

Here, because the PMF calculation requires advance knowledge of the DWC existing in water, this prerequisite should be evaluated. We studied whether the DWC can form naturally in methane solutions,[23] and although we did not find the DWC in solutions with no history of previous hydrate phases, we did find various face-saturated incomplete cages (ICs). These face-saturated ICs can encapsulate filled methane and are expected to be able to adsorb dissolved methane as does the DWC. Obviously, to study cage adsorption beginning from the DWC is the most convenient approach because the DWC has twelve uniform pentagonal faces so that the cage face effect is eliminated from the PMF calculation. Certainly, as the ubiquitous cage in different hydrate structures, the DWC is observed in systems from melted methane hydrate phases.[14–16]

In the next section, we first describe a method for calculating PMF and the simulation details. The results for the DWC–methane PMF are then given in the third section, considering the effects of four factors—the guest, the rigidity and the orientation of DWC and the interaction potential between water and methane. The most important finding is that the DWC itself strongly adsorbs the methane and the adsorption interaction is independent of the guest molecules. The significance of cage adsorption to hydrate nucleation is discussed in the fourth section, followed by a summary of the conclusions.

Methods

Potential of mean force

The potential of mean force is the free energy difference between two states along a reaction coordinate, for example the distance between DWC and methane. The PMF incorporates not only the intrinsic interactions between DWC and methane but also the effects of solvent upon them. Many methods have been proposed to obtain the PMF, such as free energy perturbation,[24] umbrella sampling,[25] weighted histogram analysis,[26] thermodynamic integration[27] and constrained molecular dynamics.[28] Here, we adopted constrained molecular dynamics. Actually, the method is a special case of the thermodynamic integration method, which calculates the PMF by integrating the derivative of the Hamiltonian, H, to the reaction coordinate, ξ,

$$PMF(\xi_2) - PMF(\xi_1) = \int_{\xi_1}^{\xi_2} \left\langle \frac{\partial H}{\partial \xi} \right\rangle d\xi. \quad (2)$$

In this work, ξ corresponds to the constrained distance between DWC and methane, r_c. Thus, $\partial H/\partial \xi$ represents the constraint force required to maintain the two groups at r_c, including both the direct interaction between them and the solvent-induced force between them. Correspondingly, $\langle \partial H/\partial \xi \rangle$ becomes the constraint mean force, $F(r_c)$, and eqn (2) becomes

$$PMF(r_2) = PMF(r_1) - \int_{r_1}^{r_2} F(r_c) dr_c, \quad (3)$$

where r_1 is the constrained distance of the reference state. When r_1 is large enough, $PMF(r_1)$ equals zero. Therefore, the PMF can be calculated from

$$PMF(r_2) = -\int_{r_1}^{r_2} F(r_c) dr_c. \quad (4)$$

Simulation details

In this work, all molecular dynamics simulations were performed with the package GROMACS.[29–32] The system was designed as a cuboid of 43.6 × 29.1 × 29.1 Å ($x \times y \times z$) and included 1240 water molecules, 1 DWC, and 2 methane molecules. The water was described by the SPC/E model[33] and the methane by the OPLS-UA potential.[34] The Lorentz–Berthelot combining rules were adopted for the cross interactions between water and methane. The Nosé–Hoover thermostat and Parrinello–Rahman barostat, with a period of 0.8 ps for both, were used to obtain the NPT ensemble with a temperature of 250 K and a pressure of 30 MPa, a state point located in the methane hydrate phase region for the above potential models.[23] The cutoff distance was 12 Å for the

Lennard–Jones potential. Periodic boundary conditions were used in all directions and the long-range interaction was calculated using the particle mesh Ewald method with a real space cutoff of 12 Å, spline order of 4 and Fourier spacing of 1.2 Å.

Initially, two groups, the DWC and the dissolved methane, were placed on the x-axis, separated by r_c. During the simulation, the two groups could move freely but r_c remained fixed. This constraint was achieved with the SHAKE algorithm. The pull codes of GROMACS[32] were used to output the constraint force between the two groups. Each simulation was run for 602 ps. The initial 2 ps were run using a time step as small as 0.2 fs to relax the system smoothly, followed by 600 ps using a time step of 1 fs. The fluctuation of system energy showed the first 102 ps was long enough to equilibrate the system. Thus, the data in the last 500 ps were averaged to get the mean force, $F(r_c)$. To obtain acceptable statistics, 20 independent runs were gathered. Thus, the configurations were sampled by each data point of $F(r_c)$ reached in 10 ns. In this work, we let r_c to take values in the range 5.0–14.0 Å with an interval of 0.2 Å. Because a distance of 14 Å is large enough, we set $r_1 = 14$ Å and PMF(14 Å) = 0 kJ mol^{-1} in eqn (3) and (4). Among the 46 data points of r_c, those with small values in the range 5.0–5.8 Å can cause abrupt abnormalities in individual runs because the forces between DWC and methane were too large. Those abnormal runs, in which the system energies were too high or the guests escaped from the DWC, could be picked out easily by comparing the system energies and guests' locations of 20 runs with each other and by visual observations. These were abandoned and re-performed starting from other initial configurations decided by random number seeds in GROMACS. However, based on such a treatment, a few data points of PMF were still unavailable. Although they did not affect the present data analysis, we will indicate them later.

Additionally, because the DWC and the dissolved methane are constrained by a separation of r_c, there is a purely entropic contribution to the PMF due to the rotation of the two groups.[32] This should be subtracted from the PMF(r_c) by $-2k_BT \ln(r_c/r_1)$. Instead, in this work, we directly corrected the raw $F(r_c)$ data by subtracting $2k_BT/r_c$, a so-called 'dynamic' term in the constraint force.[35]

Factors influencing PMF

We considered several factors that might affect the line shapes of PMF. The first factor was the cage's guest. We allowed the DWC to be filled with a methane, a water and nothing, in turn. These guests were initially placed at the DWC center and could move freely in the cage during simulations. Here, the three cage occupancies were all observed in the MD simulations on the crystal growth of methane hydrate.[17] Recently, de Pablo *et al.*[13] calculated the PMF between the DWC and a methane–water interface and found that the DWC prefers to be located at the interface on the water side. In their work, the DWC was filled with a methane with a center of mass fixed at the DWC center. By comparison, our treatment, which permitted the guests to move within the DWC, is more reasonable.

The second factor considered was cage rigidity. In this work, both a rigid and a soft DWC were studied. The rigid DWC was prepared as follows. The initial configuration of DWC was the same as in previous work.[12] In GROMACS, rigidity was obtained with a series of distance and angle constraints. The distance constraints included the length of the OH bond in water molecules being set at 1 Å, the distance between two H atoms in water at 1.633 Å and the length of H-bonds at 2.75 Å. The angle constraints included the angle between three neighboring O atoms being set at 108°, the angle of H-bonds at 0°, the tetrahedral angle of ∠HOO at 109.47° (here, the H atom does not form any H-bond in the cage), the dihedral angle of ∠OOOO and ∠HOOH in the same pentagonal face at 0° to force the O and H atoms to lie in a plane, and the dihedral angle of ∠OOOO between neighboring faces at 116.57°. These constraints were also achieved with the SHAKE algorithm and guaranteed the DWC to be quite a perfect 5^{12} cage during simulations (left side of Fig. 1). Here, we emphasized that all these angle constraints were necessary to keep cage rigidity and missing any one of them would lead to a deviation from the present one more or less. The soft DWC was obtained by keeping the distance constraints but removing the angle constraints described above. Within a few picoseconds, the initial regular DWC could relax to a soft cage that deformed and distorted continuously but maintained a water cage without breakdown (right side of Fig. 1). Evidently, in bulk water, the soft DWC is closer to the real situation than the rigid one.

The third factor considered was cage orientation. In total, four typical cases were considered: (i) the non-orientated case, meaning that the DWC could rotate freely relative to dissolved methane and no directional limit existed between them, was achieved under the constraint $r_{CM} = r_c$, where r_{CM} is the distance between the DWC center and the dissolved methane; (ii) the face-orientated case, wherein a cage face always pointed to the methane, was achieved under the constraints $r_{CM} = r_c$ and $r_{FM} = r_c - r_{CF} = r_c - 3.06$ Å, where the subscript F is the face center; (iii) the edge-orientated case, wherein a cage edge always pointed to the methane, was achieved under the constraints $r_{CM} = r_c$ and $r_{EM} = r_c - r_{CE} = r_c - 3.60$ Å, where the subscript E is the middle point of the edge; (iv) the vertex-orientated case, in which a cage vertex always pointed to the methane, was achieved under the constraints $r_{CM} = r_c$ and $r_{VM} = r_c - r_{CV} = r_c - 3.85$ Å, where the subscript V is the vertex.

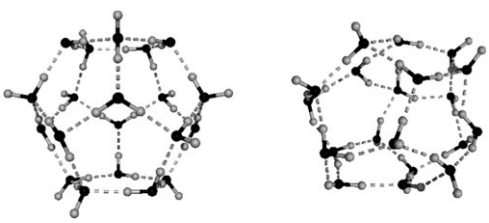

Fig. 1 Snapshots showing the typical appearances of DWC. The black balls are oxygen atoms and the grey the hydrogen. The dash lines indicate H-bonds. Left: the rigid cage, with a radius of 3.854 ± 0.002 Å, keeps its shape all the time. Right: the soft cage, with a radius of 3.786 ± 0.080 Å, changes its shape continuously over time.

Table 1 Water–methane interaction potentials used in this work[a]

	ε/kJ mol^{-1}	σ/Å
Lorentz–Berthelot (LB)	0.894299	3.4478
Konrad–Lankau (KL)[36]	1.013125	3.5600

[a] The potential equations are in the Lennard–Jones form.

We calculated the DWC–methane PMF for nine combination cases around the three factors above. They were: RD[M]$_N$M, RD[W]$_N$M, RD[0]$_N$M, SD[M]$_N$M, SD[W]$_N$M, SD[0]$_N$M, RD[M]$_F$M, RD[M]$_E$M and RD[M]$_V$M. In this notation, [] is used to intimate a polyhedral cage whose appearance is described by the characters on the left side of []—RD means the rigid DWC while SD is the soft one. Guests lie within [], with M, W and 0 meaning methane, water and the absence, respectively. On the right side of [], M is dissolved methane and the subscripts N, F, E and V mean the non-, face-, edge- and vertex-orientations of the DWC relative to the dissolved methane, respectively.

Besides the three factors above, we also evaluated the effect of the water–methane interaction potential. According to the study of Konrad and Lankau,[36] the water–methane interaction described by the Lorentz–Berthelot combining rules fails to reproduce the Henry constant observed in experiments. They proposed an optimized water–methane potential (Table 1) that can do this successfully. In this study, five cases among the nine above were repeated using the optimized water–methane potential, denoted as RD[M]$_N$M′, SD[M]$_N$M′, SD[W]$_N$M′, SD[0]$_N$M′ and RD[M]$_F$M′.

Results

RDF for the case RD[M]$_N$M

Before showing the PMF results in this work, we first compare the RDF results with previous work. Actually, the case RD[M]$_N$M was initially designed to extend our previous work in which we failed to obtain a satisfactory $g_{DWC-M}(r)$.[12] This is now shown in Fig. 2. The first sharp peak is located at the expected position (6.2 ± 0.2 Å in this work, compared with 6.15 ± 0.10 Å previously). Because the location exactly doubles the distance between the cage center and the face center (r_{CF} = 3.06 Å), it implies that the dissolved methane indeed prefers being adsorbed on one face of the DWC. The peak height is as large as 21.8 ± 2.6, meaning the existence of a very strong affinity between the DWC and methane. Additionally, the $g_{DWC-M}(r)$ in this work also shows a second peak at 10 Å, which is relatively weak, but visible. This peak corresponds to the third peak in $g_{MM}(r)$ and will be mentioned later. Compared with this work, the height of the first peak was underestimated in the previously obtained $g_{DWC-M}(r)$ and the position of the second peak, at ~10.4 Å, is approximately correct. In summary, by comparing the present and the previously obtained $g_{DWC-M}(r)$, we confirm that the first peak represents a very strong affinity between the two groups.

Because the PMF and RDF contain the same information according to eqn (1), and it is inconvenient to plot high peaks in the RDF curves, we only show the PMF results in the following.

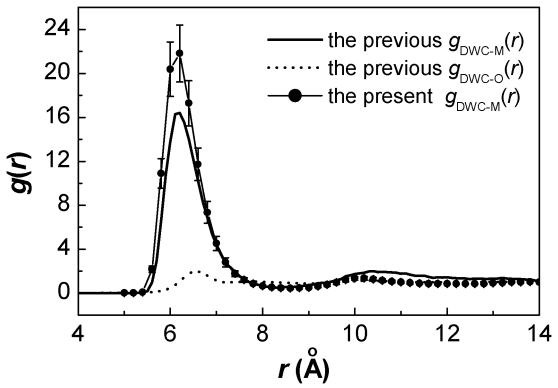

Fig. 2 Comparison of RDFs between this work and previous work.[12]

Guest effect on PMF

Fig. 3 shows the cage-methane PMF for the cases RD[M]$_N$M, RD[W]$_N$M, and RD[0]$_N$M, differing only in the guests. It is surprising that the three PMF curves are almost completely coincident. A deep well with a constant depth occurs at 6.2 Å. This is strong evidence that the rigid DWC can adsorb the dissolved methane by itself and that the attractive interaction between them is independent of guest molecules.

The activation energies for the cage–methane adsorption were calculated as the energy difference between the well at 6.2 Å and the barrier at ~8.6 Å and are listed in Table 2. They take values as large as ~8.0 kJ mol^{-1}. By comparison, the activation energy of hydrogen bonds in liquid water is about 10 kJ mol^{-1}.[37] Further, the activation energy of the contact methane pair in water is only 2.8 kJ mol^{-1}, calculated according to the methane–methane RDF in aqueous solutions.[12] Therefore, cage adsorption is a predominant interaction controlling methane's behavior, once the methane enters the vicinity of the DWC by overcoming the potential barrier.

The effect of cage rigidity on PMF

Fig. 4 shows the PMF for the soft DWC, including SD[M]$_N$M, SD[W]$_N$M, and SD[0]$_N$M. Clearly, the curves for soft DWC still show the deep wells at 6.2 Å. However, these wells are

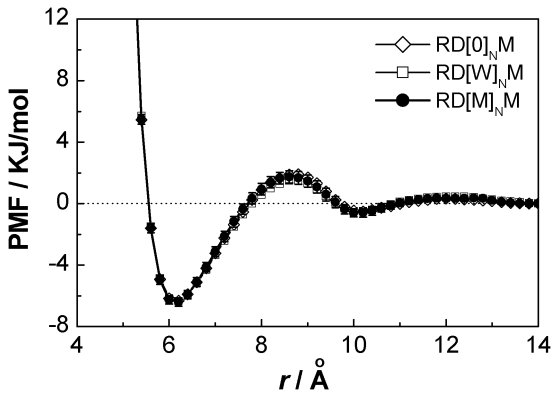

Fig. 3 The cage–methane PMFs for a rigid DWC filled with different guests. Error bars are shown only for the filled circles and those for the open symbols are obscured. Error bars are calculated according to the block average method with each block including 5 independent runs.

Table 2 Activation energies (E_a) and preferential binding coefficients ($\Gamma_{M\text{-}DWC}$) for different cases

Case	E_a/kJ mol^{-1}	Γ_{M-DWC}
RD[M]$_N$M	8.1 ± 0.4	0.43 ± 0.11
RD[W]$_N$M	7.9 ± 0.3	0.43 ± 0.08
RD[0]$_N$M	8.2 ± 0.4	0.43 ± 0.15
SD[M]$_N$M	6.3 ± 0.3	0.20 ± 0.07
SD[W]$_N$M	5.6 ± 0.3	0.21 ± 0.05
SD[0]$_N$M	5.3 ± 0.2	0.11 ± 0.04
RD[M]$_F$M	16.1 ± 0.1	9.31 [a] ± 0.54
RD[M]$_E$M		−0.13 [a] ± 0.01
RD[M]$_V$M		−0.22 [a] ± 0.03
RD[M]$_N$M′	8.9 ± 0.2	0.59 ± 0.08
SD[M]$_N$M′	6.5 ± 0.2	0.19 ± 0.06
SD[W]$_N$M′	5.9 ± 0.2	0.22 ± 0.05
SD[0]$_N$M′	6.1 ± 0.4	0.15 ± 0.07
RD[M]$_F$M′	17.0 ± 0.2	12.90 [a] ± 1.56

[a] The four $\Gamma_{M\text{-}DWC}$ values were calculated using the corresponding $g_{DWC\text{–}O}(r)$ or $g_{DWC\text{–}O}(r)'$ without limiting the DWC orientation. If considering the corresponding DWC orientations, the positive values will be larger and the negative values will be smaller than those listed. Errors were calculated according to the block average method with each block including 5 independent runs.

shallower than those of the rigid DWC. As a result, the activation energies for the soft DWC are in the range 5.3–6.3 kJ mol^{-1}, smaller than that of the rigid cage (Table 2). Here, the guest effect was checked again. One can see that these curves are very similar on the whole, except that the well depth for the empty, soft DWC is slightly smaller than that for the filled, soft DWCs. This demonstrates again that the well originates from the DWC itself rather than from the guests.

The effect of cage orientation on PMF

The cage–methane adsorption interaction showed a clear directional dependence. One can see from Fig. 5 that the curve shapes of PMF for cases RD[M]$_F$M, RD[M]$_E$M, and RD[M]$_V$M differ greatly from one another. The face-orientated DWC shows a very deep well, while the edge- and vertex-orientated DWCs do not show a complete corresponding well. This

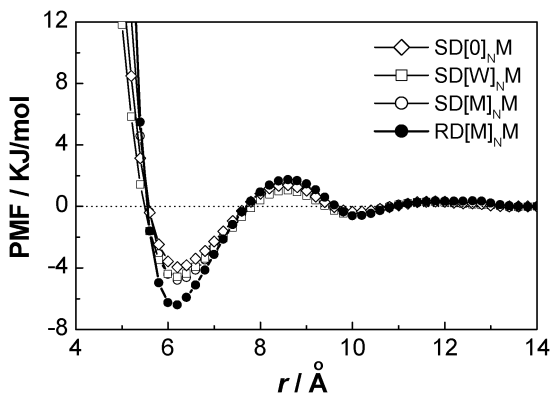

Fig. 4 The cage–methane PMFs for soft DWC containing different guests. The case RD[M]$_N$M is also plotted for comparison and, for clarity, does not show error bars. Other error bars are obscured by the symbols. The point of SD[M]$_N$M at 5.0 Å is unavailable because the guest always escapes from the soft DWC.

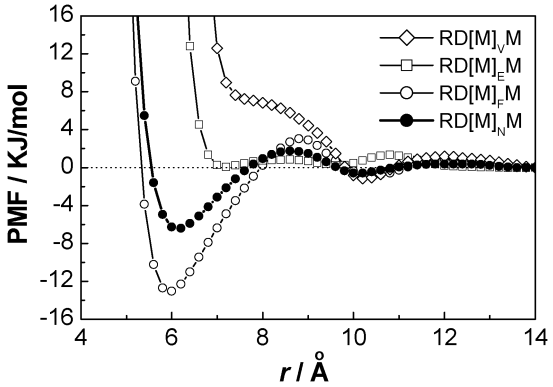

Fig. 5 As for Fig. 4 but for the rigid DWC with different orientations. The data points for RD[M]$_V$M with $r_c \leq 5.8$ Å and for RD[M]$_E$M with $r_c \leq 5.2$ Å are unavailable because the too-near constraint distances lead simulations to collapse.

phenomenon is easily understood because the vertex- and edge-orientations are the preferential positions for water molecules forming an extended, cage-like H-bonds network. The potential well for the face-orientated case is much deeper (E_a = 16 kJ mol^{-1}) and slightly nearer (at 6.0 Å) to the DWC than that for the non-orientated DWC. Because the non-orientated DWC could rotate freely, relative to dissolved methane in bulk water, the PMF for this case is actually a combination of the PMFs for the other three orientated cases. Obviously, amongst the various intermediate orientations between DWC and methane, those closest to the face-orientated case should occur with the largest likelihood and thus decide the PMF appearance of non-orientated case is similar to that of face-orientated case rather than to that of edge-orientated and vertex-orientated cases.

The water–methane potential effect on PMF

Fig. 6 shows the cage–methane PMFs for the cases RD[M]$_N$M and RD[M]$_N$M′. Compared to the former, the first well in the latter PMF is shifted towards the right and downwards, as expected because both the σ value and the ε value of the KL water–methane potential are slightly larger than those of the LB one (Table 1). This kind of relationship becomes clearer after the PMF is decomposed into two parts: a direct contribution from the interaction between DWC and methane and the solvent-induced contribution. When decomposing the PMF, the total force exerted on methane by the DWC is first calculated by

$$F_{DWC-M}(r_c) = \left\langle \sum_{i=1}^{20} \vec{F}_{O_iM} \cdot \hat{r}_{DWC-M} \right\rangle - \frac{2k_BT}{r_c}, \qquad (5)$$

where $\vec{F}_{O_iM}$ is the force vector exerted on methane by the ith oxygen atom and $\hat{r}_{DWC-M}$ is the unit vector from the DWC center to methane. The second term in the equation is for the entropy correction due to the DWC–methane constraint. After obtaining the direct DWC–methane contribution to the PMF from eqn (4) and (5), the solvent contribution is obtained immediately by subtracting this contribution from the total PMF.

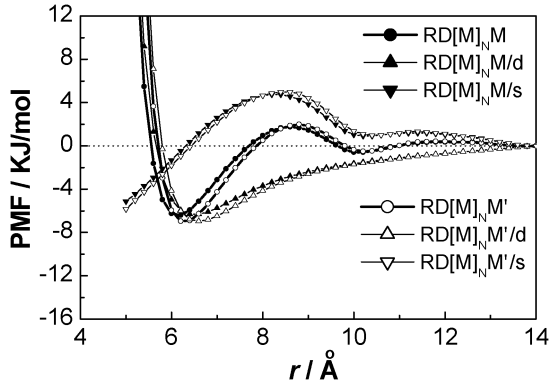

Fig. 6 Comparison of PMFs for the cases $RD[M]_NM$ and $RD[M]_NM'$. These are decomposed into the direct cage–methane contribution (/d) and the solvent-induced contribution (/s). Error bars, not shown here for clarity, are similar to those in Fig. 3, except that the error bars for the direct cage–methane contribution are obscured by the symbols.

Fig. 7 is for the face-orientated cases and shows similar features to those in Fig. 6. In particular, the difference in well depth between $RD[M]_FM$ and $RD[M]_FM'$ is 0.60 kJ mol^{-1}, exactly five times $\Delta\varepsilon$ (= 0.118826 kJ mol^{-1}, Table 1), as expected. The difference in location of the first well in the PMF curve is 0.0 Å in Fig. 6 and 0.2 Å in Fig. 7, both contrary to the expected $\Delta\sigma$ (= 0.1122 Å, Table 1). This is due to the resolution capacity of the constrained distance being as large as 0.2 Å in this work. Additionally, from the slopes of PMF curves between the wells at ~6.2 Å and the barriers at ~8.8 Å (Fig. 6 and 7), one can clearly see that the solvent-induced attractive interactions contribute largely to the total attractive interactions.

A comparison of PMF for the cases $SD[M]_NM$ and $SD[M]_NM'$ is shown in Fig. 8. Interestingly, their well depths are almost equal, against expectations, whereas the direct DWC–methane contribution to the PMF shows the expected appearance. This may be ascribed to the different solvent contribution of PMF from that in the rigid DWC cases (Fig. 6 and 7). In addition, we checked the guest effect for the soft cage cases by using the KL water–methane potential and show the results in Fig. 9. Clearly, the different guests hardly affected the PMF curves and the potential wells originate from the DWC itself, virtually independent of the guests.

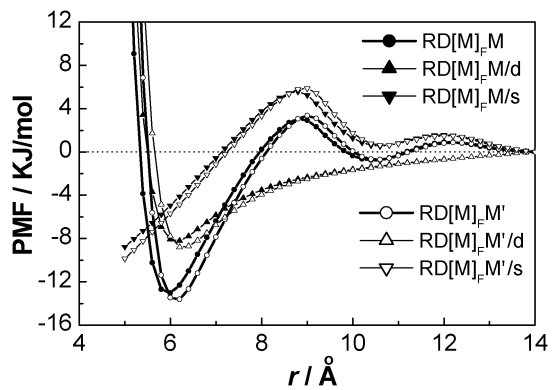

Fig. 7 As for Fig. 6 but for face-orientated cases.

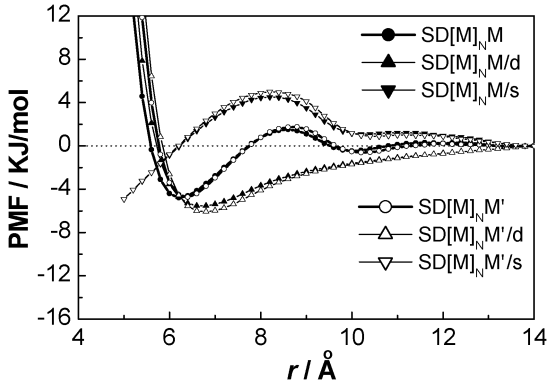

Fig. 8 The same as for Fig. 6 but for the cases $SD[M]_NM$ and $SD[M]_NM'$.

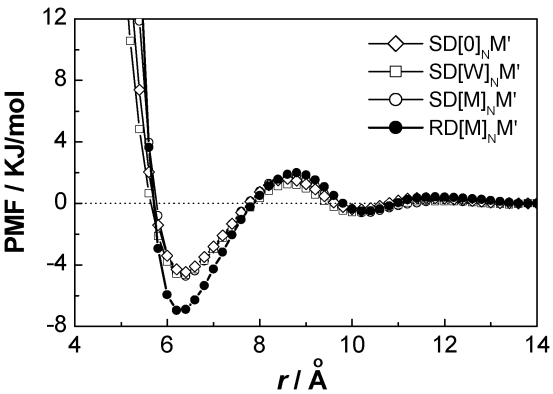

Fig. 9 The same as for Fig. 4 but for the cases using the Konrad-Lankau water–methane potential.[36]

Preferential binding coefficient

According to the preferential binding theory,[38] the affinity between DWC and methane can be described quantitatively. The theory is usually applied to the phenomenon of protein equilibria and reaction kinetics altered by co-solvents. These co-solvents can perturb the chemical potential of protein systems by associating either more strongly or more weakly with the protein than water. This phenomenon is called preferential binding. The preferential binding coefficient, Γ_{XP}, is a measure of the excess number of co-solvent molecules in the vicinity of the protein per protein molecule and it is calculated by

$$\Gamma_{XP} = \left\langle n_X^{II} - n_W^{II}\left(\frac{n_X^{I}}{n_W^{I}}\right)\right\rangle \qquad (6)$$

where n denotes the number of a specific type of molecule in a certain domain (the subscripts X, P, W represent co-solvent, protein and water, while the superscripts I and II mean the bulk domain and the protein vicinity, respectively). Baynes and Trout[38] proposed a convenient way to calculate Γ_{XP} from RDFs,

$$\Gamma_{XP} = \rho_X(\infty)\int_0^\infty (g_{PX}(r) - g_{PW}(r))\mathrm{d}V \qquad (7)$$

where $\rho_X(\infty)$ is the number density of the co-solvent far away from the protein and V is the volume.

In this work, the DWC and the dissolved methane are equivalent to the protein and the co-solvent, respectively. Thus, Γ_{M-DWC} can be calculated from the present $g_{DWC-M}(r)$ and previous $g_{DWC-O}(r)$ values (Fig. 2). The $g_{DWC-M}(r)$ values for all cases are calculated from the PMFs according to eqn (1) with $\rho_M(\infty)$ taking a value of 5.4×10^{-5} Å^{-3}, equivalent to the methane concentration (= 2 : 1262) of the systems under study. The results of Γ_{M-DWC} for the different cases are listed in Table 2. Positive values mean the affinity of methane to the DWC is larger than that of water to the DWC, and negative values are the contrary case. Obviously, the Γ_{M-DWC} results are in agreement with the above results, showing (1) that the DWC–methane affinity is stronger for rigid cages than for soft cages, (2) that the Konrad–Lankau water–methane potential leads to a slightly stronger affinity than the Lorentz–Berthelot potential, except for soft cages, (3) that the face-orientated cases show the strongest DWC–methane affinities and, (4) that the guests hardly affect DWC–methane affinity.

Discussion

Understanding the present observations

We first analyze the case of $RD[M]_NM$. Because the DWC center is actually the equilibrium position of the methane guest, the observed cage–methane PMF can be considered as a special case of the methane–methane PMF (Fig. 10). In our recent studies on the hydrophobic hydration of methane,[23] the hydration shell of methane was treated as an incomplete cage (IC), whose cage-like degree was expressed quantitatively. We found the occurrence probability of IC decreased very rapidly with increasing cage-like degree. The face-saturated ICs, which can encapsulate methane firmly, only had a probability of 10^{-4} in dilute methane solutions. Here, even if we assume the PMF between the face-saturated IC and the dissolved methane may be similar to the present PMF for the complete cage (*i.e.*, the DWC), it will not affect the usual methane–methane PMF (the thin line in Fig. 10) due to its very low weight. In most cases, the hydration shells of methane show low cage-like degree values. This means the H-bond network structures in the shells do not resemble cage structures and cannot obstruct the contact of two methanes approaching each other so that the first well at 3.9 Å occurs in the methane–methane PMF (Fig. 10). However, once a DWC (or at least a face-saturated IC) forms, it will prevent the caged methane from contacting dissolved methane through its faces so that the well at 3.9 Å cannot occur. Therefore, the cage structure originating from the hydrophobic hydration of methane changes the usual hydrophobic interaction between methanes. If the cage survives in water for a long time or, say, if the cage structure dominates the hydration shell of methane, the PMF between the caged methane and the dissolved methane will change to the present cage–methane PMF (Fig. 10). However, it is worth noting that this distinct change appears only in the short range. One can see that both the cage–methane PMF and the methane–methane PMF show similar shallow wells at about 10 Å.

Now, by treating the cage-like hydration shell of methane as an independent, long-lived macromolecule, we can conveniently explain the phenomena observed in this work. Obviously, the DWC is hydrophilic and is expected to form 20 H-bonds with solvent molecules. Because of the tetrahedral bonding pattern between water molecules, the surrounding water of DWC prefers to form an extended clathrate structure, using the DWC as a template.[39] This kind of solvent structure is exactly suited to accommodate a methane molecule in the vicinity of the DWC due to the hydrophobic hydration of methane. As a result, solvent molecules induce a strong attractive interaction between the hydrophilic DWC and the hydrophobic methane in addition to the direct attractive interaction between them. In the case of the rigid DWC, because guests cannot affect the cage structure and cannot significantly affect the solvent structure due to long distances, they do not affect the cage–methane PMF (Fig. 3). In the case of the soft DWC, the regularities of both cage and solvent structures are evidently weaker than those for the rigid DWC, thus leading the first well in the PMF to be shallower (Fig. 4 and 9). It is easy to understand the cage orientation effect on the cage–methane PMF (Fig. 5), because the vertex- and edge-orientations are ideal for the surrounding waters to occupy according to the hydrophilicity of DWC and the tetrahedral orientation of water molecules forming H-bonds.

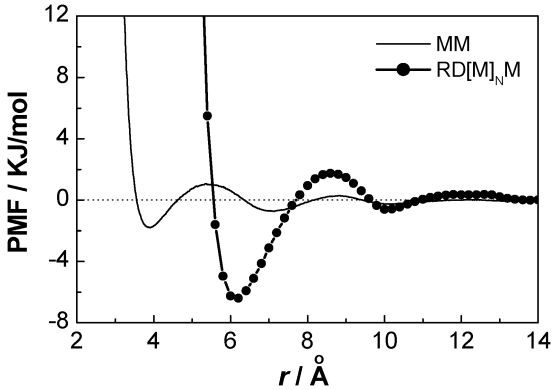

Fig. 10 The methane–methane PMF compared with the cage-methane PMF. The case MM is the methane–methane PMF, calculated from previous $g_{MM}(r)$ values in methane solutions[12] according to eqn (1).

Here, the activation energy and the preferential binding coefficient for the face-orientated case of $RD[M]_FM$ deserve further discussion. The E_a for this case is 16.1 ± 0.1 kJ mol^{-1} (Table 2), larger than the E_a of H-bonds, with about 10 kJ mol^{-1}.[37] This shows the adsorption interaction between cage and methane is stronger than the H-bond interaction between water molecules. This fact is again demonstrated by the large positive value of the preferential binding coefficient for the case $RD[M]_FM$ (Γ_{M-DWC} = 9.31). Moreover, the case of $RD[M]_FM'$ further strengthens the above fact. We have previously observed that when the DWC traps a methane, about 1.5 water molecules will be expelled from the surroundings of the DWC.[12] Usually, these expelled waters attach to the DWC faces by forming several H-bonds with some cage waters. Evidently, the strong affinity and large attractive interaction between the DWC and the dissolved methane prevents these waters competing against the methane for the positions near cage faces.

The accuracy of the present PMF calculation certainly depends on the accuracy of water–water, water–methane and methane–methane potentials because the constraint mean forces between DWC and methane, $F(r_c)$, includes DWC–methane, DWC–solvent and methane–solvent interactions. However, at present, no other report about the cage–methane PMF is available for us to make a comparison. In this work, two water–methane interaction potentials were evaluated based on the widely used SPC/E water and OPLS-UA methane models. Although PMF differences between the two water–methane potentials are evident (for example, the relative ΔE_a between $RD[M]_NM$ and $RD[M]_NM'$ is about 10%), they seem to be approximately predictable, especially for the face-orientated cases (Fig. 7).

Cage adsorption hypothesis for hydrate nucleation

Based on this work and recent progress in hydrate nucleation studies from our laboratory and others', we elucidate the cage adsorption nucleation mechanism in the following steps.

(1) *Methane dissolves into water*. It is well known that apolar molecules are almost insoluble in liquid water. Much work has been carried out to study the dissolution behaviors of apolar solutes and theories of hydrophobic effects have been proposed to describe the hydration of these solutes and the solvent-induced interactions between them.[40–43] Methane is a typical apolar molecule whose solubility in liquid water is very small ($\sim 10^{-3}$).[7] Because the solubility of methane in hydrate exceeds that in aqueous solutions 100×, the methane must aggregate in some manner before a hydrate can nucleate. In fact, in methane solutions, methane aggregation can indeed occur due to entropic driving.[21,41,44] However, this kind of aggregation favors direct methane contacts, shown by the first well at 3.9 Å in the methane–methane PMF (Fig. 10). As a result, methane bubbles, rather than the expected hydrate, form spontaneously.[45,46] Fortunately, methane contact pairs are not always favorable. When the hydration shell of a methane happens to form a cage structure, the situation is changed.

(2) *Cage forms spontaneously*. As early as 1945, Frank and Evans[47] proposed that the hydration shell of methane favors the clathrate structure, *i.e.*, the famous "iceberg model". However, since then, work from various authors seems to be inconsistent regarding whether the structure of the hydration shell is cage-like. Some authors[48,49] show it is cage-like while others[17,18] state that no cage-like hydration shell is found in methane solutions. Recently, we rechecked the hydration shells by using an incomplete cage analysis[23] and concluded that hydration shells with a high cage-like degree can form naturally but their occurrence probabilities are small and reduce very rapidly with increasing cage-like degree. An effective method to enhance their probability is to slow down the water mobility, such as lowering the system temperature and increasing the methane concentration. Although complete cages are found only in solutions with high concentrations (about 20× the normal solubility of methane), most of them are not standard hydrate cages. We emphasize that face-saturated incomplete cages have the potential to act as precursors for hydrate nucleation because these incomplete cages can encapsulate methanes as firmly as complete cages and can form naturally with a probability of $\sim 10^{-4}$ even in dilute methane solutions.

(3) *Cage adsorbs the dissolved methane*. In the present work, we showed that the DWC, relative to the dissolved methane, can provide a net attractive force field within the DWC shell, with radii between ~6.2 and ~8.8 Å. The force includes not only a direct interaction between the DWC and the methane but also solvent-induced interactions. If a methane enters the region, and happens to be roughly opposite one face of the DWC, it will be adsorbed on the DWC face with a high probability. The adsorbed methane cannot contact the caged methane directly because of the repulsion force between the adsorbed methane and the water in the cage face. Consequently, the adsorbed methane finds its equilibrium position, that is, separated from the caged methane by 6.2 Å and fenced by the cage face. This kind of face-separated methane pair is clearly different from the contact pair (3.9 Å) and solvent-separated pair (7.0 Å) commonly observed in methane solutions.[19–22] However, it is exactly the methane aggregation pattern in hydrates. Interestingly, the cage-methane attractive force depends on the cage structure itself, rather than on the guests. Hence, as long as a cage occurs in water, no matter how it forms, it possesses the ability to adsorb dissolved methane. This is the inherent driving force controlling methane aggregation towards a clathrate structure rather than a methane bubble. Certainly, the force must also control the hydrate growth at the crystal–liquid interface. We infer that the affinity between the cage at the hydrate surface and the dissolved methane should be stronger than that reported in this work because the solvent water will be affected by many surface cages and become more structural. Additionally, because the guests do not affect the cage–methane affinity, the appearance of some crystal defects, such as empty cages and water-filled cages,[17] should not further affect the growth of hydrate crystals.

(4) *Cages stabilize themselves by adsorbing more methane*. The cage formation in the hydration shell of methane is an event that has a small probability. This means that the cage is only a metastable structure in methane solutions. Its lifetime can be measured by calculating its Lindemann index.[12,13,50–52] If the cage collapses, its force field will disappear. Obviously, the longer the cage lifetime, the more opportunity it will have to capture methane. We have shown that the cage lifetime increases exponentially with the number of adsorbed methane molecules.[12] For example, the average lifetime of the DWC without adsorbing any methane is ~8 ps, and it extends to ~300 ps after adsorbing 12 methanes. This implies that the phenomenon of cage adsorbing methane is a self-assembly process. That is, the cage stabilizes itself after adsorbing a methane and then it can persist for a longer time in water so as to adsorb the next methane.

(5) *The miscellaneous growth of cages reaches an amorphous hydrate phase*. After the first cage has adsorbed a methane, the methane will also prompt its hydration shell to form another cage. At this time, the occurrence probabilities of the new cage should be larger than that of the first cage because of the existence of a shared face. Evidently, the greater the number of adsorbed methane molecules, the larger the probability that

new cages form because increasing numbers of shared faces occur between the neighboring adsorbed methanes. We have shown that a DWC adsorbing 12 methanes can develop quite regular half-cage structures in its vicinity.[12] However, just as the first cage is not always a complete cage (although it at least meets the face-saturated condition[23]), new cages may also be various face-saturated cages. Here, compared with the DWC, we assume that the face-saturated cages possess a similar affinity to methanes. Thus, new cages form and adsorb new methanes, shell by shell. As a result, methanes aggregate together with each other, separated by a clathrate H-bond network. At this stage, the network should not be an ideal hydrate structure but an amorphous phase of hydrate, *i.e.*, a miscellaneous packing of various face-saturated cages, including complete, incomplete, empty and water-filled cages. Certainly, the standard hydrate cages could also occur in the amorphous phase and even form small fragments of sI, sII, sH, and other hydrate structures. However, these fragments, if they appear, must also have a disordered distribution. Additionally, one can imagine that the new cages should grow toward the direction of the methane source so the first cage may not be the core of the amorphous packing of cages and may even disappear.

Rodger *et al.*[14,15] already observed analogous cage packing at the water–methane interface, in which the structure elements for both sI and sII even occur transitorily. They described the complex cage packing as the Ostwald step, a pre-ordered phase before the stable crystal phase. However, they believed that the processes of cage formation and methane adsorption are concurrent rather than consecutive and thus endorsed the local structuring hypothesis[11] that requires methane molecules to achieve an orderly arrangement in advance. We disagree with their viewpoint and believe they did not consider the very high concentration of methane at their water–methane interface. Their interface included about 144 methanes and 1656 waters in a volume of $36 \times 36 \times 48$ Å. Given an even distribution of these methanes, one can estimate the distance between the nearest-neighboring methanes was about 7.6 Å, less than the position ($\sim$8.8 Å) of the energy barrier in the present DWC–methane PMF. Therefore, once the hydration shell of a methane forms a cage, the nearest-neighboring methanes will feel the adsorption interaction originating from the cage immediately and would be required to diffuse only about 1.4 Å to reach their equilibrium positions ($\sim$6.2 Å). This is why the cage formation and methane adsorption seemed to occur simultaneously in their study. In other words, the local ordered arrangement of methane was not the reason for forming the cage but the consequence of its formation.

(6) *The amorphous phase transforms into a hydrate crystal.* Evidently, to obtain a perfect hydrate structure, a structural transition is required after the amorphous phase forms. Experimental evidences show that in the early stage of the formation of methane[53] and CO_2 hydrates,[54] the sII can form transiently together with sI and can transform to sI eventually. Without identifying the sII structure, other authors reported an increasing ratio of large to small cage occupancy with time for methane[55] and Xe hydrates.[56] Additionally, MD simulations showed that the sI and sII methane hydrates can transform to each other by forming $5^{12}6^3$ cages during crystal growth.[17,57] These observations imply the structural transition from the amorphous hydrate phase to the crystal hydrate phase is also possible. However, at present, it is unclear which structure, sI or sII, will develop first, what the transition pathway is and which step of formation, the amorphous phase or the following structural transition, predominantly controls the nucleation rate.

Perspective

In the above, a cage adsorption hypothesis for hydrate nucleation is proposed as several consecutive nucleation steps. Distinct from the well-known nucleation pathway described by the classical nucleation theory,[58] the hypothesis is consistent with another developing nucleation pathway,[59] which requires the formation of precursors, growth units or motifs, followed by their aggregation and the possible amorphous–crystalline transformation. At present, the first step of the hypothesis has been studied widely because of long-term interest in the hydrophobic effect. The following three steps are mainly supported by studies into the single cage[12,13,23,50–52] but more details are required in the future. For example, the cage–solute PMF requires deeper study, with consideration of the effects of various cages (especially face-saturated incomplete cages), various faces in these cages, various guest solutes and so on. The fifth step has been partly demonstrated with MD simulations at the water–methane interface by Rodger's group.[14,15] However, their system was initially prepared by melting a methane hydrate crystal and the incomplete cages, empty cages and water-filled cages in the system have not yet been thoroughly analyzed. Therefore, the water–methane interface without a hydrate history should be studied further (as is currently ongoing in our laboratory). The last step, the structural transition of the amorphous phase, remains at the stage of conjecture, despite some indirect supporting experimental evidence.[55,56]

At present, obtaining a perfect hydrate crystal in a straightforward way from a methane–water system with no history of previous hydrate phases is still unfeasible *via* MD simulations. Hence, it seems that the separate study of various nucleation-favorable events is a practical choice despite the drawback of losing the chance to obtain the full induction time. Hopefully, evaluation of the probabilities of these events may predict the hydrate nucleation rate and a study of the system's H-bond network structure by incomplete cage analysis[23] may reveal what the hydrate nucleus looks like. From this viewpoint, MD simulation is a strong tool for solving these questions. Certainly, the method of transition path sampling will also be very useful for studying these nucleation-favorable but rare events.[60,61] Additionally, elaborate experiments are expected to probe the cage structures in the early stage of hydrate formation, *i.e.*, the aqueous solution and the amorphous phase of hydrates. Apart from measuring a definite hydrate crystal,[53,54] the currently available spectroscopic techniques, such as Raman, NMR, and neutron diffraction, cannot identify cage structures[7,55,56,62] because the cages can show many different shapes, even when they are composed of the same number of water molecules. Further, the possible existence of empty cages and water-filled cages make accurate measurements difficult.

Conclusions

By using the method of constrained MD simulations, we successfully obtained the PMF between the DWC and dissolved methane for the first time. As a whole, the PMF curves are characteristic of a deep well at $\sim$6.2 Å and a shallow well at $\sim$10.2 Å, separated by a potential barrier at $\sim$8.8 Å. The deep well for the rigid DWC is deeper than that for the soft one. The guests do not affect the well depth for the rigid DWC and hardly affect that for the soft DWC. The orientation of the cage relative to the dissolved methane changes the PMF curves significantly. The PMF without considering cage orientation is a combination of the three extreme cases (*i.e.*, face-, edge- and vertex-orientated cases), and the face-orientated case dominates the basic shape of the PMF curve for the non-orientated case.

The accuracy of the PMF depends on the water–water, water–methane and methane–methane interaction potentials used. By using the SPC/E water[33] and OPLS-UA methane,[34] we evaluated two water–methane potentials described by the Lorentz–Berthelot combining rules and the Konrad–Lankau optimized potential,[36] respectively (Table 1). Similar to the KL water–methane potential having a larger σ value than the LB one, the PMF curves produced by the KL potential are also shifted slightly toward larger distances relative to those obtained with the LB potential. Apart from the soft DWC cases, the KL potential showed a larger activation energy and a stronger DWC–methane affinity than the LB one (Table 2), qualitatively reflecting the difference between the ε values of the two potentials.

The deep well in the DWC–methane PMF implies there exists a strong attractive interaction between DWC and methane, which is comparable with the hydrogen bond interaction and explains why the DWC can adsorb dissolved methane. This kind of cage adsorption interaction may be the inherent driving force that controls hydrate formation. A cage adsorption hypothesis for hydrate nucleation is thus proposed and further efforts are expected to develop it into a well-rounded theory that can reasonably predict the size and structure of a hydrate nucleus as well as the nucleation rate.

Acknowledgements

We thank Dr Zhigang Zhang for his help during this work. We also appreciate all anonymous reviewers who give us many constructive suggestions. This work is supported by the National Basic Research Program of China (the 973 Program, Grant No. 2009CB219503) and the National Natural Science Foundation of China (Grant Nos. 40672034 and 40674050).

References

1 C. A. Koh and E. D. Sloan, *AIChE J.*, 2007, **53**, 1636.
2 E. D. Sloan, *Nature*, 2003, **426**, 353.
3 C. A. Koh, *Chem. Soc. Rev.*, 2002, **31**, 157.
4 B. A. Buffett, *Annu. Rev. Earth Planet. Sci.*, 2000, **28**, 477.
5 K. A. Kvenvolden, *Proc. Natl. Acad. Sci. U. S. A.*, 1999, **96**, 3420.
6 E. D. Sloan and C. A. Koh, *Clathrate Hydrates of Natural Gases*, CRC Press Taylor & Francis Group, Boca Raton, 3nd edn, 2007.
7 W. Lu, I. M. Chou and R. C. Burruss, *Geochim. Cosmochim. Acta*, 2008, **72**, 412.
8 P. Buchanan, A. K. Soper, H. Thompson, R. E. Westacott, J. L. Creek, G. Hobson and C. A. Koh, *J. Chem. Phys.*, 2005, **123**, 164507, and many references therein.
9 E. D. Sloan and F. Fleyfel, *AIChE J.*, 1991, **37**, 1281.
10 R. L. Christiansen and E. D. Sloan, *Ann. N. Y. Acad. Sci.*, 1994, **715**, 283.
11 R. Radhakrishnan and B. L. Trout, *J. Chem. Phys.*, 2002, **117**, 1786.
12 G.-J. Guo, Y.-G. Zhang and H. Liu, *J. Phys. Chem. C*, 2007, **111**, 2595.
13 E. A. Mastny, C. A. Miller and J. J. de Pablo, *J. Chem. Phys.*, 2008, **129**, 034701.
14 C. Moon, P. C. Taylor and P. M. Rodger, *J. Am. Chem. Soc.*, 2003, **125**, 4706.
15 R. W. Hawtin, D. Quigley and P. M. Rodger, *Phys. Chem. Chem. Phys.*, 2008, **10**, 4853.
16 L. A. Báez and P. Clancy, *Ann. N. Y. Acad. Sci.*, 1994, **715**, 177.
17 J. Vatamanu and P. G. Kusalik, *J. Phys. Chem. B*, 2006, **110**, 15896; J. Vatamanu and P. G. Kusalik, *J. Phys. Chem. B*, 2008, **112**, 2399.
18 H. Nada, *J. Phys. Chem. B*, 2006, **110**, 16526.
19 L. X. Dang, *J. Chem. Phys.*, 1994, **100**, 9032.
20 W. S. Young and C. L. Brooks III, *J. Chem. Phys.*, 1997, **106**, 9265.
21 R. L. Mancera, A. D. Buckingham and N. T. Skipper, *J. Chem. Soc., Faraday Trans.*, 1997, **93**, 2263.
22 T. Ghosh, A. E. García and S. Garde, *J. Chem. Phys.*, 2002, **116**, 2480.
23 G.-J. Guo, Y.-G. Zhang, M. Li and C.-H. Wu, *J. Chem. Phys.*, 2008, **128**, 194504.
24 W. L. Jorgensen, J. K. Buckner, S. Boudon and J. Tirado-Rives, *J. Chem. Phys.*, 1988, **89**, 3742.
25 G. M. Torrie and J. P. Valleau, *J. Comput. Phys.*, 1977, **23**, 187.
26 S. Kumar, D. Bouzida, R. H. Swendsen, P. A. Kollman and J. M. Rosenberg, *J. Comput. Chem.*, 1992, **13**, 1011.
27 M. Mezei and D. L. Beveridge, *Ann. N. Y. Acad. Sci.*, 1986, **482**, 1.
28 G. Ciccotti, M. Ferrario, J. T. Hynes and R. Kapral, *Chem. Phys.*, 1989, **129**, 241.
29 H. J. C. Berendsen, D. van der Spoel and R. van Drunen, *Comput. Phys. Commun.*, 1995, **91**, 43.
30 E. Lindahl, B. Hess and D. van der Spoel, *J. Mol. Model.*, 2001, **7**, 306.
31 D. van der Spoel, E. Lindahl, B. Hess, G. Groenhof, A. E. Mark and H. J. C. Berendsen, *J. Comput. Chem.*, 2005, **26**, 1701.
32 D. van der Spoel, E. Lindahl, B. Hess, A. R. van Buuren, E. Apol, P. J. Meulenhoff, D. P. Tieleman, A. L. T. M. Sijbers, K. A. Feenstra, R. van Drunen and H. J. C. Berendsen, *Gromacs User Manual version 3.3*, www.gromacs.org, 2005.
33 H. J. C. Berendsen, J. R. Grigera and T. P. Straatsma, *J. Phys. Chem.*, 1987, **91**, 6269.
34 W. L. Jorgensen, J. D. Madura and C. J. Swenson, *J. Am. Chem. Soc.*, 1984, **106**, 6638.
35 L. Wang and J. Hermans, *J. Chem. Phys.*, 1994, **100**, 9129.
36 O. Konrad and T. Lankau, *J. Phys. Chem. B*, 2005, **109**, 23596.
37 F. W. Starr, J. K. Nielsen and H. E. Stanley, *Phys. Rev. Lett.*, 1999, **82**, 2294.
38 B. M. Baynes and B. L. Trout, *J. Phys. Chem. B*, 2003, **107**, 14058.
39 R. J. Speedy, *J. Phys. Chem.*, 1984, **88**, 3364.
40 L. R. Pratt and D. Chandler, *J. Chem. Phys.*, 1977, **67**, 3683; L. R. Pratt, *Annu. Rev. Phys. Chem.*, 2002, **53**, 409.
41 C. Pangali, M. Rao and B. J. Berne, *J. Chem. Phys.*, 1979, **71**, 2975; C. Pangali, M. Rao and B. J. Berne, *J. Chem. Phys.*, 1979, **71**, 2982.
42 N. T. Southall, K. A. Dill and A. D. J. Haymet, *J. Phys. Chem. B*, 2002, **106**, 521.
43 D. Chandler, *Nature*, 2005, **437**, 640.
44 D. E. Smith, L. Zhang and A. D. J. Haymet, *J. Am. Chem. Soc.*, 1992, **114**, 5875.
45 A. Wallqvist, *J. Phys. Chem.*, 1991, **95**, 8921.
46 O. K. Førrisdahl, B. Kvamme and A. D. J. Haymet, *Mol. Phys.*, 1996, **89**, 819.
47 H. S. Frank and M. W. Evans, *J. Chem. Phys.*, 1945, **13**, 507.
48 S. Swaminathan, S. W. Harrison and D. L. Beveridge, *J. Am. Chem. Soc.*, 1978, **100**, 5705.
49 J. Long and E. D. Sloan, *Mol. Simul.*, 1993, **11**, 145.

50 G.-J. Guo, Y.-G. Zhang, Y.-J. Zhao, K. Refson and G.-H. Shan, *J. Chem. Phys*., 2004, **121**, 1542.
51 G.-J. Guo, Y.-G. Zhang and K. Refson, *Chem. Phys. Lett*., 2005, **413**, 415.
52 G.-J. Guo, Y.-G. Zhang, M. Li and C.-H. Wu, *Proceedings of the 6th International Conference on Gas Hydrates*, (Vancouver, Canada, July 6–10), 2008, 5488.
53 J. M. Schicks and J. A. Ripmeester, *Angew. Chem., Int. Ed.*, 2004, **43**, 3310.
54 D. K. Staykova, W. F. Kuhs, A. N. Salamatin and T. Hansen, *J. Phys. Chem. B*, 2003, **107**, 10299.
55 S. Subramanian and E. D. Sloan, *Ann. N. Y. Acad. Sci*., 2000, **912**, 583.
56 I. L. Moudrakovski, A. A. Sanchez, C. I. Ratcliffe and J. A. Ripmeester, *J.Phys. Chem. B*, 2001, **105**, 12338.
57 J. Vatamanu and P. G. Kusalik, *J. Am. Chem. Soc*., 2006, **128**, 15588.
58 F. F. Abraham, *Homogeneous Nucleation Theory*, Academic Press, New York, 1974.
59 P. R. Unwin, *Faraday Discuss*., 2007, **136**, 409.
60 C. Dellago, P. G. Bolhuis, F. S. Csajka and D. Chandler, *J. Chem. Phys*., 1998, **108**, 1964.
61 P. G. Bolhuis, D. Chandler, C. Dellago and P. L. Geissler, *Annu. Rev. Phys. Chem*., 2002, **53**, 291.
62 S. F. Dec, K. E. Bowler, L. L. Stadterman, C. A. Koh and E. D. Sloan, *J. Am. Chem. Soc*., 2006, **128**, 414.